Sm and Gd isotopic shifts of Apollo 16 and 17 drill stem samples and their implications for regolith history

Hiroshi Hidaka[1]* and Shigekazu Yoneda[2]

[1]*Department of Earth and Planetary Systems Science, Hiroshima University*
Higashi-Hiroshima 739-8526, JAPAN

[2]*Department of Science and Engineering, National Science Museum*
Tokyo 169-0073, JAPAN

*corresponding author (hidaka@hiroshima-u.ac.jp)

Abstract

The isotopic compositions of Sm and Gd in lunar regolith samples from the Apollo 16 and 17 deep drill stems showed clear isotopic shifts in $^{150}Sm/^{149}Sm$ (ε= +124 to +191 for A-16, and +37 to +111 for A-17) and $^{158}Gd/^{157}Gd$ (ε= +107 to +169 for A-16, and +31 to +84 for A-17) corresponding to neutron fluences of (5.68 to 9.03)x10^{16} ncm^{-2} for A-16 and (1.85 to 5.04)x10^{16} ncm^{-2} for A-17. The depth profiles of neutron fluences suggest that the regoliths at both sites were due to incomplete mixing of three different slabs which experienced individual two-stage irradiation before and after deposition of the upper slabs. The variations in REE compositions provide chemical evidence for incompletely vertical mixing of regoliths especially at upper layers of the two sites. The thermal neutron energy index estimated from the combination of Sm and Gd isotopic shifts, defined as $\varepsilon_{Sm}/\varepsilon_{Gd}$, shows a small variation (0.61-0.64) in the A-16 core except for the surface layer. On the other hand, a large variation in $\varepsilon_{Sm}/\varepsilon_{Gd}$ = 0.67 to 0.83 in the A-17 core may result from complicated history such as two-stage irradiation and incomplete mixing during the gardening processes. Isotopic enrichments of ^{152}Gd and ^{154}Gd correlated with Eu/Gd elemental abundances and neutron fluences were also observed in almost all of fifteen samples, showing evidence of neutron capture from ^{151}Eu and ^{153}Eu, respectively.

1. Introduction

Thermalized neutrons are produced by the interaction of cosmic rays with planetary materials. Isotopes having large neutron capture cross sections such as ^{113}Cd, ^{149}Sm, ^{155}Gd and ^{157}Gd in planetary materials sensitively react with the neutrons produced near the surface of planetary bodies. Therefore, isotopic shifts of ^{114}Cd/^{113}Cd, ^{150}Sm/^{149}Sm, ^{156}Gd/^{155}Gd and ^{158}Gd/^{157}Gd in extraterrestrial materials have been used to characterize the exposure histories of lunar samples (e.g., Eugster et al., 1970; Russ et al., 1972; Curtis and Wasserburg, 1975; Sands et al., 2001). Up to the present, we have measured the isotopic compositions of Sm and Gd in terrestrial samples (Hidaka et al., 1995; Hidaka and Gauthier-Lafaye, 2001), meteorites (Hidaka et al., 1999; 2000a; 2006), and lunar samples (Hidaka et al., 2000b). In particular, the isotopic data of lunar surface samples obtained by the Apollo missions provide important information to understand the mechanism of neutron production by interaction of planetary materials with cosmic rays, because the depths of the samples are well known. Three long drilling cores of lunar regoliths were collected from the Apollo 15, 16 and 17 landing sites (hereafter A-15, -16 and –17, respectively).

Sm and Gd isotopic studies of A-15, 16 and 17 drill cores were previously performed, and the collected data were used to discuss the gardening processes on the lunar surface (Russ et al., 1972; Russ, 1973; Curtis and Wasserburg, 1975). Among the many lunar samples, A-15 drill-core samples often have been used to study the interaction of cosmic rays with regolith materials as a function of depth (e.g., Nishiizumi et al., 1997), because the A-15 regolith has not experienced major impacts in the last 500 Ma. On the other hand, the depth profiles of A-16 and A-17 neutron fluences are quite different from that of A-15 (Russ, 1973; Curtis and Wasserburg, 1975). Some models were proposed to explain the neutron fluence profiles, such as incomplete mixing of two slabs and rapid sedimentation (Russ, 1973; Curtis and Wasserburg, 1975), but additional analytical data are required for detailed discussion.

More than three decades after the first analysis of the lunar samples, the Sm and Gd isotopic compositions in the lunar long drill cores are worth repeating because of recent improvements in mass spectrometric instrumentation and chemistry procedures. Hidaka et al. (2000b) obtained new high precision Sm and Gd isotopic

compositions of A-15 samples and addressed (1) the detailed depth dependence of neutron energy spectra suggested from the combination of Sm and Gd isotopic shifts, and (2) clearly resolved isotopic enrichments of both ^{152}Gd and ^{154}Gd due to neutron capture for ^{151}Eu and ^{153}Eu, respectively. These results were already indicated in some extent in earlier studies (Russ et al., 1972), though new high precision data significantly improved quality of the discussion. In this paper, we show the newly measured Sm and Gd isotopic data of A-16 and 17 drill core samples, and construct the fine structure of neutron stratigraphy from the combination of our data with previously published data to improve the understanding of the depositional history of lunar regoliths at the A-16 and 17 sites.

2. Experimental

2.1 Samples

2.1.1. Apollo 16 core

The Apollo 16 drill core is 224 cm long. The core is divided into seven sections from 60001 (bottom) to 60007 (upper). In this study, six samples were selected from each of the individual sections except 60005. 60005 is not assigned in the core, because a part of the core corresponding to the section 60005 located between 60 and 100 cm deep from the surface was originally missing. Although the A-16 core may not be suitable for the study of neutron stratigraphy, because it lacks a part of the core, it is nevertheless interesting to compare the isotopic data of the A-16 samples with those of A-15 and A-17 core samples. Isotopic analyses of Sm and Gd in the A-16 samples were initially performed by Russ (1973) for the study of interaction between cosmic rays and the lunar surface. It is known that the A-16 core shows the highest neutron fluences among lunar materials. Because the Gd and Sm data from 60002 and the Sm data of 60006 have not been reported in the previous works (Russ, 1973), in this study we completely measured a pair of Sm and Gd isotopic ratios from all sections of the core except 60005.

2.1.2. Apollo 17 core

Nine samples were selected from the 284 cm deep drill core of the Apollo 17 landing site. The core is divided into nine sections from 70001 (bottom) to 70009

(upper). The upper 20 cm of the A-17 core corresponding to 70009 is well mixed in the layer, which is known as a reworked zone. Curtis and Wasserburg (1975) already measured the isotopic abundances of Sm and Gd of the A-17 samples. Among the A-17 samples, Sm isotopic data from the 70002, 70004, 70005, 70007 and 70009 layers have not been studied yet. Here, we report the Sm and Gd isotopic data of the A-17 samples from all nine layers including the Sm data of 70002, 70004, 70005, 70007 and 70009 samples.

2.2 Chemical procedures

Prior to the isotopic work, a new method of chemical separation of lighter rare earth elements (LREE) including Sm and Gd was developed. For the isotopic analysis, effective separation of the target element from isobaric interferences is required. Cation exchange chromatography has been often used for mutual REE separation (Lugmair and Marti, 1971; Hidaka et al., 1988). However, the previous REE separation method using a cation exchange resin in ammonia form with α-hydroxy isobutyric acid (α-HIBA) as an eluent requires complicated processes for the conditioning of the resin and for the purification of α-HIBA (Hidaka et al., 1995).

In this study, the elution behavior of LREE was calibrated using a lanthanide-specific resin (LN resin) commercially manufactured by Eichrom Technologies Inc. and then the technique was applied for the mutual separation of Sm and Gd in the lunar samples. This resin comprises di-(2-ethylhexyl)-phosphoric acid (HDEHP) loaded on a polymeric substrate (Pin and Zalduegui, 1997).

20-30 mg of each sample was digested by HF-$HClO_4$. The sample was then taken to dryness and redissolved in 1 mL of 2M HCl. The solution was divided into two portions: the main portion for Sm and Gd isotopic measurements and the rest for the determination of REE abundances. The sample solution was loaded onto a cation exchange resin column (Bio-rad AG50WX8, 200-400 mesh, H^+ form, 50 mm length, 4.0 mm i.d.) and washed with 4.7 mL of 2M HCl before REE were eluted with 3 mL of 6M HCl. This REE fraction from the first column was evaporated until dry and redissolved in a drop of 0.1M HCl. The solution was loaded onto a second column packed with LN resin (particle size of 100-150 μm, 100 mm length, 2.5 mm i.d.) to

separate Nd, Sm and Gd using 0.25M, 0.35M and 0.5M HCl, respectively. The recovery rate of each element through this procedure is more than 90%. The total procedural blanks of Sm and Gd were less than 100 pg for each element. The elution behaviors of Nd, Sm, Eu and Gd are illustrated in Fig. 1. This method using LN resin is more convenient and simpler than the previous method using α-HIBA .

Another aliquot of the sample solution was used for the determination of REE abundances by inductively coupled plasma mass spectrometry (ICP-MS).

2.3 Mass Spectrometry

A VG54-30 thermal ionization mass spectrometer equipped with seven Faraday cup collectors was used in this study. Details of mass spectrometric techniques for Sm and Gd isotopic analyses were previously reported (Hidaka et al., 1995). More than $8x10^{-12}$ A of $^{152}Sm^{+}$ ion and $5x10^{-12}$ A of $^{158}Gd^{+}$ ion currents were detected from each sample. Correction for instrumental mass fractionation was performed using an exponential law with normalization to $^{147}Sm/^{154}Sm$ and $^{156}Gd/^{160}Gd$.

Sm isotopic ratios have been generally normalized using $^{147}Sm/^{152}Sm= 0.56081$ (Russ et al., 1972). However, in the case of lunar surface samples, there is a possibility that ^{152}Sm is produced by thermal neutron capture on ^{151}Eu. The use of $^{147}Sm/^{152}Sm$ may not be suitable for normalization of neutron-irradiated samples. Instead of $^{147}Sm/^{152}Sm$, $^{147}Sm/^{154}Sm=0.65918$ was also used for the normalization of lunar samples (Russ, 1973: Curits and Wasserburg, 1975). We recalculated our Sm isotopic data using $^{147}Sm/^{154}Sm=0.65918$ normalization, and did not find detectable excess of ^{152}Sm for the A-16 and A-17 samples. This is consistent with low Eu/Sm elemental ratios (0.18 to 0.23) of all of the samples used in this study.

In the past Gd isotope studies, $^{156}Gd/^{160}Gd= 0.9361$ has been generally used for normalization (e.g., Eugster et al., 1970). In the case of neutron-irradiated samples, $^{156}Gd/^{160}Gd$ ratio cannot be fixed to a constant value because of the isotopic shift from ^{155}Gd to ^{156}Gd. In order to solve this problem, Hidaka et al. (1995) applied modified $^{156}Gd/^{160}Gd$ ratio ($0.9361+\alpha$) by the iteration of ^{155}Gd and ^{156}Gd isotopic shifts and instrumental mass fractionation, assuming that a depletion of ^{155}Gd is equal to an enrichment of ^{156}Gd. From the isotopic data for non-irradiated material, the sum of $^{155}Gd/^{160}Gd$ and $^{156}Gd/^{160}Gd$ isotopic ratios is fixed to 1.61290. The α values in

individual samples are determined when the normalization by $^{156}Gd/^{160}Gd$= 0.9361+α leads to $^{155}Gd/^{160}Gd$= 0.67680-α (Hidaka et al., 1995).

ICP-MS (VG Plasma Quad III) was used for the determination of REE contents in individual samples. The analytical conditions of ICP-MS were the same as those used by Shinotsuka et al. (1995).

3. Results and discussion

The isotopic compositions of Sm and Gd of A-16 and A-17 samples are shown in Table 1. The analytical uncertainties in the table are 2σ of the means. All of the samples from A-16 and A-17 show significantly large isotopic shifts of $^{150}Sm/^{149}Sm$ and $^{158}Gd/^{157}Gd$. Figure 2 shows diagrams of isotopic shifts for (a) $^{149}Sm/^{152}Sm$ vs. $^{150}Sm/^{152}Sm$, and (b) $^{157}Gd/^{160}Gd$ vs. $^{158}Gd/^{160}Gd$. It is well known from previous studies that the A-15 drill core is the best to study the interaction of cosmic rays with lunar surface materials, because the stratigraphic order of the site has not been disturbed by regolith gardening (Russ et al., 1972; Nishiizumi et al., 1997; Hidaka et al., 2000b). For comparison, In Fig. 2, the isotopic data points from the A-15 samples are also plotted together with those of A-16 and A-17 samples analyzed in this study. In the case of isotopic variations due to neutron capture reactions, the depletions of ^{149}Sm and ^{157}Gd abundances quantitatively correspond to the enrichments of ^{150}Sm and ^{158}Gd, respectively. Therefore, all of the samples in Fig. 2 should plot on neutron-capture lines with slopes of -1. Our normalization method for Gd isotopic compositions works well, because all of the corrected Gd data points lie on the neutron capture line in Fig. 2. This is a very important point when studying neutron energy spectra on the lunar surface, because the combination of Sm and Gd isotopic shifts defined as $\varepsilon_{Sm}/\varepsilon_{Gd}$ provides information on thermalized neutron energy (Lingenfelter et al., 1972).

3.1. Depth profile of isotopic variations of Sm and Gd

3.1.1. $^{150}Sm/^{149}Sm$ and the $^{158}Gd/^{157}Gd$

Because the amounts of Sm and Gd isotopic shifts correspond to the neutron fluences caused by cosmic-ray irradiation of the samples, there are several methods of estimating the neutron fluences from the Sm and Gd isotopic data (Eugster et al., 1970; Russ et al., 1972; Hidaka et al., 1995). The depth profiles of the $^{150}Sm/^{149}Sm$ and

$^{158}Gd/^{157}Gd$ isotopic shifts from both drill cores look remarkably similar. In particular, detailed discussion of the neutron depth profile is made possible by combining Sm data sets from this work and previous studies by Russ (1973) and Curtis and Wasserburg (1975). Both data sets use the same normalization procedure, based on $^{147}Sm/^{152}Sm$= 0.56081. The depth profile of $^{150}Sm/^{149}Sm$ are generally consistent with previous studies, even if none of our samples were collected from the exactly same depth with previous studies. The unit of depth in Fig. 3 is expressed as g cm^{-2}, considering the difference in the density of individual sections of the cores. Density data, 1.47 to 1.75 g cm^{-3} for A-16 and 1.74 to 1.99 g cm^{-3} for A-17, were cited from Carrier (1974). Neutron fluence profiles with fine-scaled depth resolution for the A-16 and A-17 cores can be constructed from the combination of two Sm data sources, which makes it possible to discuss the depositional history of regoliths at the individual sites. Three processes, complete mixing, continuously accreting, and continuously eroding, modify the undisturbed neutron-capture depth profile in the core (Russ et al., 1972).

If the regolith layers have not been mixed for a long time, the profile of neutron fluence can be shown as a function of depth fitted with a single curve. The A-15 core is a good example to observe the depth dependence of neutron fluence (Russ et al., 1972; Hidaka et al., 2000b). The A-15 profile was constructed from the interaction of cosmic rays with a slab undisturbed for 450 Ma on top of a well-mixed layer having 450-500 Ma irradiation. The A-15 profile shows an asymmetric curve with a maximum at approximately 190 g cm^{-2} depth. Based on the A-15 profile, neutron capture depth profile of undisturbed single slab has a well-defined shape with a FWHM of 310 to 330 g cm^{-2} (Lingenfelter et al., 1972; Kornblum et al., 1973). On the other hand, as shown in Fig. 3, the A-16 and A-17 drill-core profiles show more than two maxima apparently consisting of three curves.

For the A-16 profile, Russ (1973) proposed a continuous accretion model or a two-slab irradiation model. Reconsidering a continuous accretion model from our new Sm data together with previous data, there are discrete points at 60001 and 60002. However, as shown in Fig. 3(A), a two-slab model provides a better fitting of the combination of two Sm data points.

Curtis and Wasserburg (1975) provided a detailed depth profile of the A-17

drill-core from ten different Gd data points. Their Gd data show a flatter profile between 200-500 g cm^{-2} than those of Sm shown in Fig. 3(B), and were attributed to accretion processes. The results from the A-17 Gd data in earlier work seem inconsistent with the Sm data in this work. To address this issue, our Gd data also should be compared with those in earlier works (Russ, 1973; Curtis and Wasserburg, 1975), although the normalization procedures for instrumental mass fractionation of Gd isotopes are different between two data sets. Figures 4(A) and 4(B) show the $^{158}Gd/^{157}Gd$ isotopic variations with depth for the A-16 and A-17 drill-cores, respectively. The Gd data of the A-16 samples provides a similar depth profile to that of the Sm data shown in Fig. 3 (A). On the other hand, as shown in Fig. 4(B), there are some discontinuous points between two data sets for the A-17 samples at upper (0 to 100 g cm^{-2}) and lower (473 to 535 g cm^{-2}) layers. Since the Sm data of 70008.189 and 70008.221 samples were not reported by Curtis and Wasserburg (1975), the reason for the disparities at the upper layer of the A-17 Gd profile is unclear. However, judging from the agreement between two data sets at middle layers (170 to 400 g cm^{-2}), it is concluded that significant isotopic differences are not artificially produced from the difference of normalization procedures. Therefore, large deviation between neighboring two samples, 70002,467 from this study and 70002,9 should be accepted as a peculiar property of the A-17 drill-core.

In both cases for the A-16 and A-17 drill-cores shown in Figs. 3 and 4, the Sm and Gd profiles have more than two peaks, and it is impossible to explain such profiles only from the irradiation of a single slab plus accretion and vertical mixing. To address this issue, a two-slab model for the evolution of the regolith has been proposed (Russ, 1973). We also assumed the multi-slab model for the A-16 and A-17 profiles, and applied curve fitting to the individual profiles. The results are shown as solid lines in Figs. 3 and 4. The resulting curve with a solid line in each figure is the sum of the three curves separately shown as two dotted lines. Fitting the data allows us to consider the following features of the two sites.

A-16: In order to fit the discontinuous data points between 225 and 250 g cm^{-2} and below 350 g cm^{-2}, three slabs having individual irradiation records are required for the A-16 drill core. Since the existence of the oldest slab (>360 g cm^{-2}) is supported by

only one data point (60001,8), its irradiation record and depositional history cannot be well defined. Russ (1973) reported two possibilities for the boundary between first and second slab, 165 and 235 g cm^{-2}. In this study, the closest fit is obtained by setting the boundary of middle and upper slabs between 225 and 250 g cm^{-2}. The middle slab having an initial fluence Ψ_0 = (3.9 to 4.5)x10^{16} n cm^{-2} deposited 850 to 940 Ma ago. The upper slab was deposited 580 Ma ago with Ψ_0 = 5.5x10^{16} n cm^{-2}. Upper <80 g cm^{-2} layer was added after deposition of slab3, which appears well-mixed from the Sm profile, but the Gd profile suggests heterogeneous mixing of the present surface with upper slab.

A-17: The discontinuities of the A-17 profile from 180 to 236 g cm^{-2} and from 473 to 535 g cm^{-2} are also explained by three-slab model. Three data points from 70001,9, 70001,77 and 70002,467 scatter below 500 g cm^{-2}, which suggest incomplete mixing near the boundary between two slabs. The middle slab was deposited 680 Ma ago with Ψ_0 = 0.93x10^{16} n cm^{-2}. A broad shape of slab2 cannot be explained only from irradiation on an undisturbed slab, considering an expected neutron fluence profile with a FWHM of 310 to 330 g cm^{-2} (Lingenfelter et al., 1972; Kornblum et al., 1973). Both the Sm and Gd profiles in this study suggest that slab2 consists of two components, irradiation on an undisturbed slab from 299 to 473 g cm^{-2} and a rapid addition of 235 to 299 g cm^{-2} layer after deposition of the slab2. The slab3 was deposited 440 Ma ago with Ψ_0 = 1.3x10^{16} n cm^{-2}. The upper <90 g cm^{-2} layer was added after deposition of slab3, and incomplete mixing occurred in the upper layer.

These results may have uncertainties because of the restricted number of samples available for the sites, and more isotopic data from the deeper site (>400 g cm^{-2} for A-16 and >500 for A-17 g cm^{-2}) are required for detailed discussion. Slight deviations between analytical data points and the calculated curve suggest that the profiles were constructed not only by irradiation of undisturbed slabs but also by partial accretion and mixing processes. However, it is difficult to quantitatively consider the contribution of individual processes only from the depth profile of neutron fluences. If the irradiated slabs had been disturbed by later events, variations in chemical components and neutron energy spectra in the cores would be expected. Therefore, we use the data from neutron energy spectra and REE abundances, and discuss the

contribution of surface processes toward the deposition of regoliths in a later section.

3.1.2. Neutron capture of ^{151}Eu and ^{153}Eu

As shown in Table 1(b), isotopic excesses of ^{152}Gd and ^{154}Gd are also observed in almost all of the A-16 and A-17 samples. Considering the neutron capture cross sections of ^{151}Eu (5.8×10^{-21} cm^{-2}) and ^{153}Eu (3.8×10^{-22} cm^{-2}), one of the major reasons for the ^{152}Gd and ^{154}Gd enrichments is neutron-captured production from ^{151}Eu and ^{153}Eu, respectively. The neutron-capture production yields of ^{152}Gd and ^{154}Gd depend on the neutron fluence and isotopic abundances of ^{151}Eu and ^{153}Eu, respectively, because the production rates are determined by the term $N\sigma\Psi$; where N is the number of target isotopes, σ is the neutron capture cross section, and Ψ is the neutron fluence. It is expected that the multiplication of neutron fluence (Ψ) and ^{151}Eu/^{152}Gd and ^{153}Eu/^{154}Gd isotopic ratios (N) linearly correlate with the isotopic ratios ^{152}Gd/^{160}Gd and ^{154}Gd/^{160}Gd, respectively, if the neutron capture reactions dominantly occurred in ^{151}Eu and ^{153}Eu. The data are shown in Figure 5. The data of the A-15 samples (Hidaka et al., 2000b) are also plotted together with those of the A-16 and A-17 samples.

The total production rates of neutron capture produced ^{150}Sm and ^{158}Gd are not influenced by chemical fractionation, because the parent and daughter isotopes belong to the same element. In this case, quantitative discussion of the neutron fluence is possible from the isotopic data alone. On the other hand, ^{152}Gd and ^{154}Gd are not produced from Gd, but from Eu isotopes. Therefore, any elemental disturbance such as chemical fractionation and addition of foreign materials by bombardment results in the isotopic disequilibrium between ^{151}Eu-^{152}Gd and ^{153}Eu-^{154}Gd. The data of the A-15 site may be a good reference to understand the isotopic equilibrium between Eu and Gd, because the A-15 site is believed to have been little disturbed by major impacts in the last 500 Ma.

Figures 5(A) and 5(B) show diagrams for neutron capture reactions of ^{151}Eu(n,$\gamma\beta^-$)^{152}Gd and ^{151}Eu(n,$\gamma\beta^-$)^{152}Gd. The ^{152}Gd and ^{154}Gd isotopic enrichments show proportional variations with $N\Psi$, which quantitatively suggests that the isotopic excesses of ^{152}Gd and ^{154}Gd are due to neutron capture reactions from ^{151}Eu and ^{153}Eu, respectively. However, in Fig. 5(A), different correlation trends can be seen between

the A-16 and A-17 samples, which are caused by the difference in the macroscopic neutron capture cross-section as a result of different chemical compositions of the samples. Lingenfelter et al. (1972) reported a variation of the effective neutron capture cross section of ^{151}Eu as a function of the chemical composition of the target material. Details on the chemical compositions of the samples used in this study are described in later section 3.3. Using the chemical composition data of individual samples, neutron capture cross sections of ^{151}Eu are calculated as 5000 to 5900 barn for A-16 and 7500 to 8000 barn for A-17. The expected correlations for the A-16 and A-17 samples are shown as shaded zones in Fig. 5(A). Except for the three data points (60003, 60004 and 60006) for A-16 and the two (70004 and 70009) for A-17, measured ^{152}Gd isotopic excesses are in good agreement with the calculated values. Considering the location of the five outliers, 60006 (approximately 5 g cm^{-2} depth from the surface), 60004 (near interface between slab2 and 3 shown in Figs. 3(A) and 4(A)), 60003 (interface between slab2 and 3), 70004 (upper edge of slab2) and 70009 (10 g cm^{-2} depth from the surface), these five samples might have been incompletely mixed with neighboring regoliths.

The correlation profile of ^{154}Gd excesses in Fig. 5(B) is simpler than that of ^{152}Gd in Fig. 5(A), because the neutron capture cross section of ^{153}Eu does not sensitively vary with the chemical composition. As shown in Fig. 5(B), the ^{154}Gd excesses observed in this study are in agreement with calculated values for neutron-capture on ^{153}Eu. There is a possibility that ^{138}Ba^{16}O interferes with ^{154}Gd on the mass spectra. However, the monitoring signals at mass regions of approximately 150 (^{150}Sm and ^{134}Ba^{16}O) and 153 (^{137}Ba^{16}O) during the Gd isotopic analyses showed little contribution of isobaric mass interferences such as ^{152}Sm^{+}, ^{136}Ba^{16}O^{+} and ^{138}Ba^{16}O^{+} onto ^{152}Gd and ^{154}Gd mass spectra.

REE data shown in a later section also support the chemical difference between shallower samples (60006, 70008 and 70009) and other samples in the A-16 and A-17 sites. The isotopic excesses of ^{150}Sm and ^{158}Gd quantitatively correspond to the accumulation of the neutron irradiation, because both of the neutron capture reactions, ^{149}Sm(n,γ)^{150}Sm and ^{157}Gd(n,γ)^{158}Gd, occur as isotopic shifts within a single element. Therefore, even if a large chemical fractionation among REE had occurred during the regolith evolution, the isotopic shifts for ^{150}Sm/^{149}Sm and ^{158}Gd/^{157}Gd remain closed

systems. On the other hand, neutron-capture produced ^{152}Gd and ^{154}Gd are not produced from Gd isotopes but from Eu isotopes via β^- decay. It is quite plausible that the addition of different materials into a shallow layer disturbed the neutron capture profiles of ^{151}Eu-^{152}Gd and ^{153}Eu-^{154}Gd in the two sites. However, as shown in Fig. 5(B), these disturbances are not clear in the ^{153}Eu-^{154}Gd depth profile because of the relatively large analytical uncertainties. Because ^{152}Gd isotopic abundance is more than ten times lower than that of ^{154}Gd, compositional variations in the drill-core samples may sensitively affect the ^{152}Gd isotopic abundance.

3.2. REE abundance patterns

REE abundance patterns of A-15 regolith are strongly affected by those of KREEP (Hidaka et al., 2000b), meanwhile regolith samples from A-16 and A-17 show individually different features in the REE patterns. The REE patterns may provide a hint to identify the major provenances of the individual regolith sites. C1 chondrite-normalized REE patterns of all samples from A-16 and A-17 sites are shown in Fig. 6.

The REE patterns of seven samples from 70001 (deepest) to 70007 in the A-17 core resemble those of high-Ti and high-K mare basalts, which show convex-upward patterns with large negative Eu anomalies (BVSP, 1981). On the other hand, the REE patterns from two shallower sections, 70009 and 70008, are evidently different from those of seven other samples in the A-17 core. Significant depletion of LREE (La to Nd) is observed in the patterns of 70009 and 70008, although the shapes of HREE (Sm to Lu) of both samples are very similar to those of seven other samples. The result suggests that the sections from 70001 to 70007 are well mixed by earlier gardening processes, but that the shallow sections 70008 and 70009 are contaminated with other materials by later impacts. According to previous REE studies, some high-Ti mare basalts of the A-17 site, such as 75055 and 70017, have LREE depletions with slight convex-upward patterns, although their negative Eu anomalies are smaller than those of 70008 and 70009 (BVSP, 1981). For the detailed discussion of REE geochemistry in the A-17 core, three parameters, namely, total REE concentrations (ΣREE) expressed by ppm, Eu negative anomaly (parameterized by Eu/Eu*= Eu/(Sm+Gd)/2), and chemical fractionation between LREE and HREE (LREE/HREE), were used in this study.

Figure 7 shows diagrams of Eu/Eu* vs. ΣREE and LREE/HREE vs. ΣREE. For comparison, data points of major types of rocks collected from the A-17 site were also plotted in Fig. 7 (Hubbard et al., 1974; Rhodes et al., 1974; Simonds, 1975; Wänke et al., 1975; Blanchardt et al.,1975; 1976; 1977; Ryder and Norman, 1979; BVSP, 1981). As far as REE are concerned, the A-17 regoliths are dominated by high-Ti mare basalts. In addition, contribution of impact melt breccias or fragmental breccias may also affect the REE components of the core.

The REE patterns of all of the six A-16 samples are similar in the core, which show the enrichment of LREE and the depletion of HREE with negative Eu anomalies. The patterns are similar to those of the different types of rock collected from the A-16 site (Brunfelt et al., 1973; Hubbard et al., 1973; 1974; Haskin et al., 1973; Wänke et al., 1975; Lindstrom et al., 1977; Lindstrom and Lindstrom, 1986; Borchardt et al., 1986). Figure 8 shows diagrams of Eu/Eu* vs. ΣREE and LREE/HREE vs. ΣREE for the A-16 drill stem samples. The data from different types of rock collected from the A-16 site are also plotted in the same figures. The data points of the A-16 core samples are explained using a two- or three-component mixing model that consists of granulitic melt breccia, Mg-rich breccia, or monomict ferroan anorthosite. The data of both LREE/HREE vs. ΣREE and Eu/Eu* vs. ΣREE diagrams reveal that the chemical properties of the drill-core samples are strongly affected by the several types of breccia at this site. In addition, judging from the lack of significant variation in REE pattern among the six samples in the A-16 core shown in Fig. 6, the regolith is well mixed in the core.

3.3. Neutron energy spectra

The neutron energy spectra has been characterized by a parameter, $\varepsilon_{Sm}/\varepsilon_{Gd}$, dependent on the difference in the neutron capture resonances of ^{149}Sm (0.0973 eV) and ^{157}Gd (0.0314 eV). Lingenfelter et al. (1972) predicted neutron energy spectra as a function of the chemical compositions of target materials and temperature. The comparison of the $\varepsilon_{Sm}/\varepsilon_{Gd}$ data between measured values (Russ et al., 1972; Russ, 1973; Curtis and Wasserburg, 1975) and theoretical values (Lingenfelter et al., 1972) suggests that the lunar neutron spectrum includes a higher energy component than the

theoretically calculated values for 200 K.

An examination of the depth dependence of $\varepsilon_{Sm}/\varepsilon_{Gd}$ is an important aspect of this study. Previous measurements of $\varepsilon_{Sm}/\varepsilon_{Gd}$ in the A-16 and A-17 cores did not reveal a change in energy spectrum with depth, although the effect may have been masked by the experimental uncertainties (Russ, 1973; Curtis and Wasserburg, 1975). Only the A-15 stem drill samples are considered to be suitable to study the depth dependence, because it has preserved a clear depth profile of neutron irradiation records without disturbance. Our previous data of the A-15 core show a significant difference in $\varepsilon_{Sm}/\varepsilon_{Gd}$ between the lower layer and the upper layer in the core, which suggests a depth dependence of the neutron energy spectrum (Hidaka et al., 2000b). As shown in Table 2, the $\varepsilon_{Sm}/\varepsilon_{Gd}$ values from the A-16 and A-17 sites indicate variations greater than analytical uncertainties even in the same drill-cores.

3.3.1. Dependence on chemical composition

The chemical composition of the target defined as an effective total macroscopic neutron capture cross section, Σ_{eff} (cm^2 g^{-1}), is needed for the detailed discussion of neutron energy spectra (Lingenfelter et al., 1972). The $\varepsilon_{Sm}/\varepsilon_{Gd}$ values in individual cores show distinctively different ranges, 0.75-0.79 for A-15, 0.61-0.64 for A-16 and 0.74-0.82 for A-17, mainly due to differences in chemical compositional (Fig. 9). On the basis of the previously determined Σ_{eff} data for A-15 (Hidaka et al., 2000b) and A-17 (Curtis and Wasserburg, 1975), the $\varepsilon_{Sm}/\varepsilon_{Gd}$ values are plotted as a function of the individual Σ_{eff} data in Fig. 9 to confirm the relationship between neutron energy spectra and chemical compositions. The Σ_{eff} data for A-16 were calculated from major element abundances of average composition of A-16 soils (Heiken et al., 1991) and REE data measured in this study (Table 3), because there are no references of the Σ_{eff} data for A-16. Calculated $\varepsilon_{Sm}/\varepsilon_{Gd}$ values with three different energies, 200 K, 300 K and 400 K (Lingenfelter et al., 1972), are also plotted in Fig. 9.

Figure 9 shows that the large difference in $\varepsilon_{Sm}/\varepsilon_{Gd}$ between the A-16 core and the other two cores is mainly due to the difference in chemical composition. The data from the A-17 sites show a large variation in neutron energy, even if the dependence of chemical composition is considered. The samples from 70002, 70004, 70008 and

70009 show significantly lower $\varepsilon_{Sm}/\varepsilon_{Gd}$ than the other five samples, which lie in the 300-400 K temperature range together with the A-15 and A-16 samples. The data show the complicated irradiation history of the A-17 core, which suggests the incomplete mixing of the regolith between the original slab and the later deposited material. On the other hand, the variation in $\varepsilon_{Sm}/\varepsilon_{Gd}$ data from the A-16 is smaller than that of A-17, and almost all of the data points lie on the 300 K line.

3.3.2. Depth dependence

In general, except for a few cases such as 15001 and 15002 in the A-15 drill-core, the Σ_{eff} values are very similar to those of a regolith-core. Assuming similar chemical compositions in the single core, the depth dependence of thermal neutron energy on the lunar surface will be discussed. Figure 10 illustrates the variation of $\varepsilon_{Sm}/\varepsilon_{Gd}$ as a function of depth in the A-16 and A-17 cores. For comparison, the data of the A-15 core are also shown in the same figure. As shown in Fig. 10, the data of the A-15 samples in early work suggest that the neutron energy spectrum has a depth dependence of neutron energy, and that it is better thermalized at sample 15004 having the highest neutron fluences in the A-15 drill-core. (Hidaka et al., 2000b).

Sample 60007 from the upper layer in A-16 might have been mixed by numerous bombardments near the surface. Therefore, the neutron energy spectra seen by the core might have been affected by several irradiation stages. Except for the shallowest sample 60007, there is no large variation in $\varepsilon_{Sm}/\varepsilon_{Gd}$ (0.611-0.644) in the A-16 core. A small $\varepsilon_{Sm}/\varepsilon_{Gd}$ variation observed in 60001 to 60006 apparently shows a depth dependence of the neutron energy spectrum similar to that observed in the A-15 core (Hidaka et al., 2000b). Among the five samples, deeper three samples 60001 to 60003 have experienced at least two-stage neutron irradiation, at the deposition of the middle slab and after the deposition of the upper slab as shown in Figs 3(A) and 4(A). If the depth dependence like the A-15 core is observed in the middle slab of the A-16 core, sample 60001 with the highest fluence should have the lowest $\varepsilon_{Sm}/\varepsilon_{Gd}$ variation. However, later irradiation after the deposition of the upper slab have affected the $\varepsilon_{Sm}/\varepsilon_{Gd}$ values of the middle slab.

The profile of A-17 shows a different trend from those of A-15 and A-16.

Samples 70009 and 70008 from shallower layers may include several irradiation records caused by mixing near the surface. A large difference in REE pattern between the two shallow samples and the others, as shown in Fig. 6, also supports the significant mixing effect near the surface in the A-17 core. Except for the two data sets from the shallow layer, a discontinuity in the $\varepsilon_{Sm}/\varepsilon_{Gd}$ variation is observed at the depths of 70004 (326 g cm^{-2}) and 70002 (510 g cm^{-2}) in the A-17 core. Considering a three-slab model for the A-17 core shown in Figs. 3(B) and 4(B), an irradiation of the potential slab during the gardening processes might have caused a discontinuity in the depth profile of $\varepsilon_{Sm}/\varepsilon_{Gd}$. The data sets from samples 70005 to 70007, which are located in the middle slab, have experienced two-stage neutron irradiation, at the deposition of the middle slab and after the deposition of the upper slab. In addition, the data of 70002 and 70006 result from mixing of two components, which is plausible since they are located at the boundaries of individual slabs. Therefore, it is not simple to discuss the depth dependence of neutron energy spectrum of the A-17 samples. In particular, we cannot find sufficient interpretation from our current data to explain the low $\varepsilon_{Sm}/\varepsilon_{Gd}$ of four samples, 70002,70004,70008 and 70009 from our current data. However, previous studies may provide some hints for the interpretation. Curits and Wasserburg (1975) found a peculiar property in the materials from 70008 observed in the Gd isotopes and the spallogenic ^{126}Xe data, and concluded that the sample consists of two components, highly irradiated materials in the deep site and lightly irradiated materials in the shallow site. This is consistent with the result from the track density analysis by Crozaz et al. (1974). Therefore, the variation of $\varepsilon_{Sm}/\varepsilon_{Gd}$ in the A-17 core might have occurred independent of the depth as a result from migration of lightly irradiated materials in the deep site. In addition, exact determination of the macroscopic cross section values (Σ_{eff}) from the chemical composition data of the A-17 samples is also required for further discussion of the depth-dependence of $\varepsilon_{Sm}/\varepsilon_{Gd}$ values.

4. Conclusions

Isotopic analyses of Sm and Gd for the A-16 and A-17 drill-cores provide information on the neutron stratigraphy and regolith history on the lunar surface. Our isotopic data are consistent with the results of previous studies (Russ,1973; Curtis and

Wasserburg, 1975). Detailed neutron fluence profiles with depth in the A-16 and A-17 cores can be constructed from the combined data from previous studies and this study.

The isotopic data lead to the following findings and probabilities on the regolith processes at the A-16 and the A-17 sites.

(1) The depth profiles of the neutron fluences suggest the irradiation of three slabs, at both sites. The existence of the oldest slab is supported by discontinuous data points from lower layers (>350 g cm^{-2} for A-16 and >500 g cm^{-2} for A-17), but it is not conclusive because of the restricted number of samples from deeper layers. The data points located at the boundary between two slabs deviate from the fitting curve, which is due to two-stage irradiation and vertical mixing during the gardening processes.

(2) It is not simple to discuss the depth dependence of neutron energy spectrum from the isotopic data of the A-16 and A-17 samples, because several samples in the drill-cores might have experienced two-stage irradiation and incompletely vertical mixing. The profiles of $\varepsilon_{Sm}/\varepsilon_{Gd}$ values in two sites do not reflect irradiation of a single, undisturbed slab.

(3) The samples from the shallow layer in the cores show a different irradiation history from other deeper layers, because the layers near the surface have been influenced by later bombardments and mixed with additional materials having different chemical compositions from original regoliths. REE abundance data also support the migration of additional materials into the shallow layer of the A-16 core.

(4) Significant isotopic enrichments of ^{152}Gd and ^{154}Gd reflect the neutron-capture production by $^{151}Eu(n,\gamma\beta^-)^{152}Gd$ and $^{153}Eu(n,\gamma\beta^-)^{154}Gd$, respectively. The degrees of isotopic excess of ^{152}Gd and ^{154}Gd are consistent with the neutron capture production rates calculated from the neutron fluences and Eu isotopic abundances.

Acknowledgments

The A-16 and 17 regolith samples were provided by NASA Johnson Space Center in response to sample request No. 2420. We thank Y. Takahashi for his help with the ICP-MS analysis. Critical comments and suggestions by J.R. DeLaeter, K. Welten, N. Kita and an anonymous journal reviewer were very helpful to improve the first draft of the manuscript. This study was financially supported by a Grant-in-Aid for Scientific Research of Japan Society for the Promotion of Science (No. 17204051 to H.H.).

References

Blanchard, D.P., Haskin, L.A., Jacobs, J.W., Brannnon, J.C., Korotev, R., 1975. Major and trace element chemistry of Boulder 1 at Station 2, Apollo 17. *The Moon* **14,** 359-371.

Blanchard, D.P., Jacobs, J.W., Brannnon, J.C., Haskin, L.A., 1976. Major and trace element composition of matrix and aphaniticclastsfromconsortiumbreccia 73215. *Proc. Lunar Sci. Conf.* **7,** 2179-2187.

Blanchard, D.P., Jacobs, J.W., Brannnon, J.C., 1977. Chemistry of ANT-suite and felsite clasts from consortium breccia 73215 and of gabbroic anorthosite 79215. *Proc. Lunar Sci. Conf.* **8,** 2507-2524.

Borchardt, R., Stöffler, D., Spettel, B., Palme, H., Wänke, H., Wacker, K., Jessberger, E.K., 1986. Composition, structure, and age of the Apollo 16 subregolith basement as deduced from the chemistry of post-Imbrium melt bombs. *J. Geophys. Res.* **91,** E43-E54.

BVSP (Basaltic Volcanism Study Project), 1981. In *Basaltic Volcanism on the Terrestrial Planets.* Pergamon, New York. 1286 pp.

Brunfelt, A.O., Heier, K.S., Nilssen, B., Sundvoll, B., Steinnes, E., 1973. Geochemistry of Apollo 15 and 16 materials. *Proc. Lunar Sci. Conf.* **4,** 1209-1218.

Carrier, W.D., 1974. Apollo drill core depth relationship. *The Moon* **10**, 183-194.

Crozaz, G., Drozd, R., Hohenberg, C., morgan, C., Ralston, C., Walker, R., Yuhas, D., 1974. Lunar surface dynamics: Some general conclusions and new results from Apollo 16 and 17. *Proc. Lunar Sci. Conf.* **5,** 2475-2499.

Curtis, D.B., Wasserburg, G.J., 1975. Apollo 17 neutron stratigraphy – sedimentation and mixing in the lunar regolith. *The Moon* **13**, 185-227.

Eugster, O.,. Tera, F., Burnett, D.S., Wasserburg, G.J., 1970. Isotopic composition of gadolinium and neutron-capture effects in some meteorites. *J. Geophys. Res.* **75**, 2753-2768.

Haskin, L.A., Helmke,P.A.,Blanchard,D.P.,Jacobs,J.W.,Telunder,K.,1973. Major and trace element abundances in samples from the lunar highlands. *Proc. Lunar Sci. Conf.* **4,** 1275-1296.

Heiken, G.H., Vaniman, D.T., French, B.M., 1991. In *Lunar sourcebook: a user's guide to the moon.* Cambridge University Press. 736pp.

Hidaka, H., Gauthier-Lafaye, F., 2001. Neutron capture effects on Sm and Gd isotopes in uraninites. *Geochim. Cosmochim. Acta* **65**, 941-949.

Hidaka, H., Masuda, A., Fujii, I., Shimizu, H., 1988. Abundance of fissiogenic and pre-reactor natural rare-earth elements in a uranium ore sample from Oklo. *Geochem. J.* **22**, 47-54.

Hidaka, H., Ebihara, M., Shima, M., 1995. Determination of the isotopic compositions of samarium and gadolinium by thermal ionization mass spectrometry. *Anal. Chem.* **34**, 1437-1441.

Hidaka, H., Ebihara, M., Yoneda, S., 1999. High fluences of neutrons determined from Sm and Gd isotopic compositions in aubrites. *Earth Planet. Sci. Lett.* **173**, 41-51.

Hidaka, H., Ebihara, M., Yoneda, S., 2000a. Isotopic study of neutron capture effects on Sm and Gd in chondrites. *Earth Planet. Sci. Lett.* **180**, 29-37.

Hidaka, H., Ebihara, M., Yoneda, S., 2000b. Neutron capture effects on Sm, Eu and Gd in Apollo 15 deep drill core samples. *Meteoritics & Planetary Science* **35**, 581-589.

Hidaka, H., Yoneda, S., Marti, K., 2006. Regolith history of the aubritic meteorite parent body revealed by neutron capture effects on Sm and Gd isotopes. *Geochim. Cosmochim. Acta* **70,** 3449-3456.

Hubbard, N.J., Rhodes, J.M., Gast, P.W., Bansal, B.M., Shih, C.-Y., Wiesmann, H., Nyquist, L.E., 1973. Lunar rock types: the role of plagioclase in non-mare and highland rock types. *Proc. Lunar Sci. Conf.* **4,** 1297-1312.

Hubbard, N.J., Rhodes, J.M., Wiesmann,H.,Shih,C.-Y.,Bansal,B.M.,1974.The chemical definition and interpretation of rock types returned from the non-mare regions of the Moon. *Proc. Lunar Sci. Conf.* **5,** 1227-1246.

Kornblum J.J., Fireman, E.L., Levine, M., Aronson, A., 1973. Neutrons in the moon. *Proc. Lunar Sci. Conf.* **4,** 2171-2182.

Lindstrom, M.M., Lindstrom, D.J., 1986. Lunar granulites and their precursor anorthositic norites of the early lunar crust. *J. Geophys. Res.* **91,** D263-

D276.

Lindstrom, M.M., Nava, D.F., Lindstrom, D.J., Winzer, S.R., Lum, R.K.L., Schuhmann, P.J., Schuhmann, S., Philpotts, J.A., 1977. Geochemical studies of the white breccia boulders at North Ray Crater, Descartes region of the lunar highlands. *Proc. Lunar Sci. Conf.* **8,** 2137-2151.

Lingenfelter, R.E., Canfield, E.H., Hampel, V.E., 1972. The lunar neutron flux revisited. *Earth Planet. Sci. Lett.* **16**, 355-369.

Lugmair, G.W., Marti, K., 1971. Neutron capture effects in lunar gadolinium and the irradiation histories of some lunar rocks. *Earth Planet. Sci. Lett.* **13**, 32-42.

Nishiizumi, K., Fink, D., Klein, J., Middleton, R., Masarik, J., Reedy, R.C., 1997. Depth profile of ^{41}Ca in an Apollo 15 drill core and the low-energy neutron flux in the Moon. *Earth Planet. Sci. Lett.* **148**, 545-552.

Pin, C., Zalduegui , J.F.S., 1997. Sequential separation of light-rare-earth elements, thorium and uranium by miniaturized extraction chromatography: Application to isotopic analyses of silicate rocks. *Anal. Chim. Acta*, **339**, 79-89.

Rhodes, J.M., Rodgers, K.V., Shih, C., Bansal,B.M.,Nyquist,L.E.,Wiesmann,H., Hubbard, N.J., 1974. The relationship between geology and soil chemistry at the Apollo 17 landing site. *Proc. Lunar Sci. Conf.* **5,** 1097-1117.

Russ, G.P., 1973. Apollo 16 neutron stratigraphy. *Earth Planet. Sci. Lett.* **19**, 275-289.

Russ, G.P., Burnett, D.S., Wasserburg, G.J., 1972. Lunar neutron stratigraphy. *Earth Planet. Sci. Lett.* **15**, 172-186.

Ryder, G., Norman, M.D., 1979. Catalog of Pristine Non-Mare Materials Part 1. Non-Anorthosites (Revised). JSC Publ. No. 14565, NASA Johnson Space Center, Houston. 147 pp.

Sands,, D.G., De Laeter, J.R., Rosman, K.J.R., 2001. Measurements of neutron capture effects on Cd, Sm and Gd in lunar samples with implications for the neutron energy spectrum. *Earth Planet. Sci. Lett.* **186**, 335-346.

Shinotsuka, K., Hidaka, H., Ebihara,M.,1995. Detailed abundances of rare earth elements, thorium and uranium in chondritic meteorites: An ICP-MS study. *Meteoritics* **30**, 694-699.

Simonds, C.H., Warner, J.L., Phinney, W.C., 1975. The petrology of the Apennine Front revisited (abstract) In *Lunar Science VI*, pp.744-746.

Wänke, H., Palme, H., Baddenhausen, H., Dreibus, G., Jagoutz, E., Kruse, H., Palme, C., Spettel, B., Teshke, F., Thacker, R., 1975. New data on the chemistry of lunar samples: Primary matter in the lunar highlands and the bulk composition of the Moon. *Proc. Lunar Sci. Conf.* **6,** 1313-1340.

Table 1

(a) Isotopic compositions of Sm

sample	$^{144}Sm/^{152}Sm$	$^{148}Sm/^{152}Sm$	$^{149}Sm/^{152}Sm$	$^{150}Sm/^{152}Sm$	$^{154}Sm/^{152}Sm$
STD	0.114957 ± 1	0.420442 ± 5	0.516872 ± 4	0.275980 ± 3	0.850854 ± 7
A-16					
60001,98	0.114959 ± 8	0.420484 ± 17	0.513455 ± 16	0.279406 ± 20	0.850849 ± 43
60002,740	0.114961 ± 9	0.420478 ± 18	0.513475 ± 18	0.279349 ± 19	0.850883 ± 35
60003,611	0.114958 ± 10	0.420490 ± 13	0.513884 ± 16	0.278965 ± 15	0.850823 ± 33
60004,669	0.114963 ± 16	0.420431 ± 35	0.513697 ± 35	0.279154 ± 30	0.850827 ± 48
60006,415	0.114966 ± 12	0.420423 ± 17	0.514608 ± 15	0.278183 ± 14	0.851032 ± 29
60007,511	0.114655 ± 13	0.420622 ± 40	0.514644 ± 28	0.278196 ± 26	0.850806 ± 41
A-17					
70001,77	0.114966 ± 6	0.420465 ± 7	0.515079 ± 7	0.277774 ± 5	0.850830 ± 12
70002,467	0.114964 ± 9	0.420449 ± 8	0.514835 ± 8	0.277951 ± 6	0.850903 ± 14
70003,544	0.114977 ± 10	0.420463 ± 12	0.514942 ± 12	0.277879 ± 9	0.850891 ± 16
70004,579	0.114971 ± 7	0.420458 ± 12	0.515233 ± 13	0.277617 ± 9	0.850867 ± 22
70005,490	0.114976 ± 5	0.420481 ± 8	0.515256 ± 8	0.277574 ± 7	0.850838 ± 13
70006,511	0.114974 ± 9	0.420474 ± 12	0.515302 ± 14	0.277491 ± 11	0.850889 ± 21
70007,457	0.114978 ± 13	0.420425 ± 15	0.515092 ± 15	0.277741 ± 13	0.850897 ± 24
70008,522	0.114971 ± 10	0.420427 ± 8	0.516166 ± 8	0.276626 ± 6	0.850858 ± 13
70009,557	0.114963 ± 7	0.420432 ± 7	0.516066 ± 7	0.276698 ± 6	0.850889 ± 13

Errors are 2σ of mean.

The data are normalized to $^{147}Sm/^{152}Sm=0.56081$.

(b) Isotopic compositions of Gd

sample	$^{152}Gd/^{160}Gd$	$^{154}Gd/^{160}Gd$	$^{155}Gd/^{160}Gd$	$^{156}Gd/^{160}Gd$	$^{157}Gd/^{160}Gd$	$^{158}Gd/^{160}Gd$
STD	0.009270 ± 8	0.099747 ± 2	0.676872 ± 5	0.9361	0.715878 ± 4	1.135846 ± 7
A-16						
60001,98	0.009388 ± 32	0.099774 ± 28	0.673513 ± 40	0.939387	0.708541 ± 35	1.143242 ± 27
60002,740	0.009360 ± 32	0.099788 ± 30	0.673580 ± 39	0.939320	0.708611 ± 54	1.143202 ± 65
60003,611	0.009313 ± 27	0.099788 ± 25	0.674027 ± 38	0.938873	0.709335 ± 55	1.142452 ± 62
60004,669	0.009317 ± 28	0.099774 ± 25	0.673812 ± 32	0.939088	0.708688 ± 60	1.143060 ± 77
60006,415	0.009307 ± 32	0.099742 ± 30	0.674592 ± 39	0.938308	0.710888 ± 63	1.140835 ± 51
60007,511	0.009347 ± 27	0.099739 ± 22	0.675072 ± 27	0.937828	0.711238 ± 36	1.140519 ± 50
A-17						
70001,77	0.009340 ± 25	0.099747 ± 20	0.675174 ± 29	0.937726	0.712857 ± 17	1.138887 ± 22
70002,467	0.009361 ± 10	0.099757 ± 10	0.673732 ± 38	0.939168	0.712251 ± 56	1.139450 ± 48
70003,544	0.009361 ± 27	0.099755 ± 28	0.674282 ± 29	0.938618	0.712510 ± 13	1.139218 ± 18
70004,579	0.009319 ± 26	0.099754 ± 30	0.675250 ± 49	0.937650	0.712827 ± 40	1.138825 ± 49
70005,490	0.009380 ± 29	0.099748 ± 38	0.676062 ± 14	0.936838	0.713053 ± 12	1.138569 ± 15
70006,511	0.009337 ± 11	0.099750 ± 9	0.674742 ± 11	0.938158	0.713253 ± 19	1.138414 ± 25
70007,457	0.009350 ± 6	0.099762 ± 6	0.675150 ± 10	0.937750	0.712914 ± 14	1.138741 ± 23
70008,522	0.009306 ± 19	0.099743 ± 14	0.675625 ± 20	0.937275	0.714615 ± 16	1.137055 ± 18
70009,557	0.009269 ± 20	0.099733 ± 18	0.675957 ± 12	0.936943	0.714509 ± 11	1.137167 ± 12

Errors are 2σ of mean.

The data are normalized to (^{155}Gd + ^{156}Gd) /^{160}Gd=1.61290.

Table 2 Sm and Gd isotopic shifts and parameters for neutron capture effects of A-16 and A-17 samples

sample	Depth (cm)	Depth (g/cm^2)	$^{150}Sm/^{149}Sm$	$^{158}Gd/^{157}Gd$	$^{158}Gd/^{157}Gd$	Ψ ($x10^{16}$ ncm^{-2})	$\varepsilon_{Sm}/\varepsilon_{Gd}$
STD			0.533943 ± 7	1.38298 ± 1	1.58664 ± 1		
A-16							
60001,98	218.8-219.3	342.7-343.6	0.544168 ± 42	1.39476 ± 8	1.61352 ± 9	9.03 ± 0.04	0.644±0.010
60002,740	183.9-184.4	281.6-282.5	0.544036 ± 42	1.39452 ± 8	1.61330 ± 15	8.95 ± 0.06	0.641±0.012
60003,611	164.6-165.1	249.4-250.2	0.542856 ± 34	1.39293 ± 8	1.61060 ± 15	8.04 ± 0.06	0.630±0.013
60004,669	131.0-131.5	194.7-195.4	0.543422 ± 69	1. 39369 ± 7	1.61292 ± 17	8.82 ± 0.06	0.611±0.016
60006,415	33.5-34.2	48.7-49.6	0.540573 ± 31	1.39093 ± 8	1.60480 ± 15	6.10 ± 0.05	0.617±0.017
60007,511	3.5-4.0	5.1-5.8	0.540560 ± 58	1.38923 ± 6	1.60357 ± 10	5.68 ± 0.03	0.661±0.020
A-17							
70001,77	287.8-288.3	525.6-526.5	0.539284 ± 12	1.38887 ± 6	1.59764 ± 5	4.15 ± 0.02	0.820±0.004
70002,467	278.7-279.2	509.8-510.7	0.539884 ± 14	1.39398 ± 8	1.59998 ± 14	5.04 ± 0.06	0.752±0.008
70003,544	215.2-216.7	395.6-398.3	0.539632 ± 22	1.39203 ± 6	1.59888 ± 4	4.62 ± 0.02	0.785±0.004
70004,579	176.2-177.7	324.9-326.6	0.538818 ± 22	1.38860 ± 10	1.59762 ± 11	4.15 ± 0.04	0.750±0.008
70005,490	162.3-163.3	298.1-299.9	0.538711 ± 16	1.38573 ± 3	1.59675 ± 3	3.82 ± 0.02	0.796±0.004
70006,511	128.2-128.7	235.4-236.3	0.538502 ± 26	1.39040 ± 2	1.59609 ± 6	3.57 ± 0.03	0.815±0.007
70007,457	91.4-91.9	170.2-171.0	0.539207 ± 30	1.38895 ± 2	1.59730 ± 4	4.03 ± 0.02	0.833±0.006
70008,522	49.3-50.3	95.3-97.4	0.535924 ± 14	1.38727 ± 4	1.59162 ± 4	1.88 ± 0.02	0.673±0.008
70009,557	5.6-6.1	9.9-10.7	0.536168 ± 14	1.38610 ± 2	1.59154 ± 3	1.85 ± 0.01	0.768±0.007

Ψ values were calculated from the $^{158}Gd/^{157}Gd$ ratios by the following equation,

$$\Psi = \frac{(^{158}Gd/^{157}Gd)_{sample} - (^{158}Gd/^{157}Gd)_{STD1}}{(^{158}Gd/^{157}Gd)_{STD2} - (^{158}Gd/^{157}Gd)_{STD1}} \times \frac{\sigma_{STD2}}{\sigma_{sample}} \times (1.40 \times 10^{16})$$

where σ_{sample}=(1.0 to 1.1)x10^5 barn for A-16, and (7.9 to 8.0)x10^4 barn for A-17, σ_{STD2}=9.7x10^4 barn

$(^{158}Gd/^{157}Gd)_{STD1}$=1.58664±0.00001, $(^{158}Gd/^{157}Gd)_{STD2}$=1.59109±0.00001 from Hidaka et al. (1995)

$\varepsilon_{Sm}/\varepsilon_{Gd}$ is defined as the following equation,

$$\frac{\varepsilon_{Sm}}{\varepsilon_{Gd}} = \frac{\dfrac{(^{150}Sm/^{149}Sm)_{sample} - (^{150}Sm/^{149}Sm)_{STD}}{1 + (^{150}Sm/^{149}Sm)_{sample}}}{\dfrac{(^{158}Gd/^{157}Gd)_{sample} - (^{158}Gd/^{157}Gd)_{STD}}{1 + (^{158}Gd/^{157}Gd)_{sample}}}$$

Table 3 REE abundances (ppm) of A-16 and A-17 samples

	La	Ce	Pr	Nd	Sm	Eu	Gd	Tb	Dy	Ho	Er	Tm	Yb	Lu	ΣREE	Eu/Eu*	LREE/HREE
A-16																	
60001,98	12.4	33.1	4.48	20.0	5.58	1.13	6.49	1.15	7.00	1.43	4.23	0.592	3.97	0.558	102.1	0.569	2.20
60002,740	11.1	29.2	3.95	17.8	5.00	1.04	5.99	1.05	6.44	1.33	3.91	0.549	3.60	0.549	91.5	0.578	2.08
60003,611	9.14	24.3	3.35	15.0	4.24	0.935	4.94	0.863	5.36	1.11	3.25	0.458	3.03	0.442	76.5	0.619	2.09
60004,669	11.4	30.6	4.30	19.5	5.46	1.19	6.38	1.11	7.09	1.44	4.16	0.590	3.98	0.606	97.8	0.610	2.00
60006,415	5.40	13.9	1.94	8.63	2.40	0.553	2.98	0.499	3.13	0.651	1.85	0.262	1.74	0.295	44.2	0.629	2.01
60007,511	10.2	26.6	3.66	16.1	4.52	0.945	5.26	0.920	5.83	1.19	3.41	0.485	3.22	0.512	82.8	0.587	2.11
A-17																	
70001,77	8.81	24.0	3.71	18.6	6.21	1.13	8.37	1.46	9.22	1.98	5.48	0.760	5.00	0.798	95.6	0.476	1.25
70002,467	9.09	25.0	3.83	19.3	6.87	1.43	9.05	1.60	10.4	2.13	6.23	0.846	5.62	0.818	102.3	0.551	1.19
70003,544	10.2	27.3	4.06	20.1	6.89	1.36	8.74	1.53	9.93	2.04	5.95	0.826	5.41	0.779	105.1	0.534	1.35
70004,579	8.98	24.2	3.67	18.2	6.33	1.41	8.23	1.45	9.45	1.93	5.71	0.779	5.16	0.752	96.3	0.592	1.26
70005,490	9.65	27.4	4.26	21.8	7.76	1.52	10.6	1.90	12.4	2.57	7.62	1.06	7.08	1.05	116.7	0.509	1.03
70006,511	9.36	26.0	3.89	19.2	6.65	1.36	8.64	1.51	9.87	2.02	5.92	0.815	5.35	0.767	101.3	0.546	1.29
70007,457	9.34	25.9	3.93	20.1	7.14	1.45	9.47	1.67	10.8	2.20	6.46	0.876	5.80	0.843	105.9	0.534	1.19
70008,522	9.12	28.4	4.94	27.9	11.2	2.26	16.8	2.98	20.0	4.11	12.0	1.65	11.0	1.62	153.9	0.501	0.699
70009,557	7.54	22.6	3.63	19.5	7.53	1.59	10.3	1.82	12.0	2.44	7.14	0.978	6.45	0.945	104.5	0.546	0.927

Figure captions

Fig. 1. Elution behaviors of Nd, Sm, Eu and Gd using LN resin with HCl as an eluent.

Fig. 2. Diagrams of three-isotope plots for (a) $^{149}Sm/^{152}Sm$ vs. $^{150}Sm/^{152}Sm$, and (b) $^{157}Gd/^{160}Gd$ vs. $^{158}Gd/^{160}Gd$. A-15 data are from Hidaka et al. (2000b). The solid line in each figure indicates the neutron capture line. The analytical uncertainties of individual data points are within the symbols.

Fig. 3. Depth profiles of $^{150}Sm/^{149}Sm$ in (a) A-16 core and (b) A-17 core. The solid line in each figure depicts the fitting curve. Reference data are from Russ (1973) for A-16 and from Curtis and Wasserburg (1975) for A-17.

Fig. 4. Depth profiles of $^{158}Gd/^{157}Gd$ in (a) A-16 core and (b) A-17 core. The solid line in each figure depicts the fitting curve. Reference data are from Russ (1973) for A-16 and from Curtis and Wasserburg (1975) for A-17.

Fig. 5. Correlation diagrams for (A) $^{151}Eu/^{160}Gd \cdot \Psi$ vs. $^{152}Gd/^{160}Gd$, and (B) $^{153}Eu/^{160}Gd \cdot \Psi$ vs. $^{154}Gd/^{160}Gd$. Shaded zones in Fig. 5(A) indicate the expected correlation values. Considering that the neutron capture cross section of ^{151}Eu has a dependence on the chemical composition of the sample, the expected neutron capture production rates of ^{152}Gd were calculated from the cross section of the reaction

$^{151}Eu(n,\gamma\beta^{-})^{152}Gd$ as a function of chemical composition (Σ_{eff}) defined by Lingenfelter et al. (1972). A solid line in Fig. 5(B) indicates the expected correlation line using a cross section of 330 barn for the reaction $^{153}Eu(n,\gamma\beta^{-})^{154}Gd$. The error bars of the individual data points are from analytical uncertainties given as 2 σ of the mean.

Fig. 6. C-1 chondrite-normalized REE abundance patterns of A-16 and A-17 core samples.

Fig. 7. Correlation diagrams for (a) ΣREE vs. Eu/Eu*, and (b) ΣREE vs. LREE/HREE of A-17 samples. Reference data are from literature (Hubbard et al., 1974; Rhodes et al., 1974; Simonds, 1975; Wänke et al., 1975; Blanchardt et al.,1975; 1976; 1977; Ryder and Norman, 1979; BVSP, 1981)

Fig. 8. Correlation diagrams for (a) ΣREE vs. Eu/Eu*, and (b) ΣREE vs. LREE/HREE of A-16 samples. Reference data are from literature (Brunfelt et al., 1973; Hubbard et al., 1973; 1974; Haskin et al., 1973; Wänke et al., 1975; Lindstrom et al., 1977; Lindstrom and Lindstrom, 1986; Borchardt et al., 1986)

Fig. 9. Diagram for compositional dependence (Σ_{eff}) of neutron energy ($\varepsilon_{Sm}/\varepsilon_{Gd}$) of A-16 and A-17 samples. The data of A-15 are from Hidaka et al. (2000b). The three types of line in the figure show the neutron energy spectra at three different temperatures, 200, 300 and 400 K, predicted by Lingenfelter et al. (1972).

Fig. 10. Variation of neutron energy ($\varepsilon_{Sm}/\varepsilon_{Gd}$) of A-16 and A-17 with depth (g cm^{-2}). The data of A-15 are from Hidaka et al. (2000b).

Fig. 1 Hidaka and Yoneda

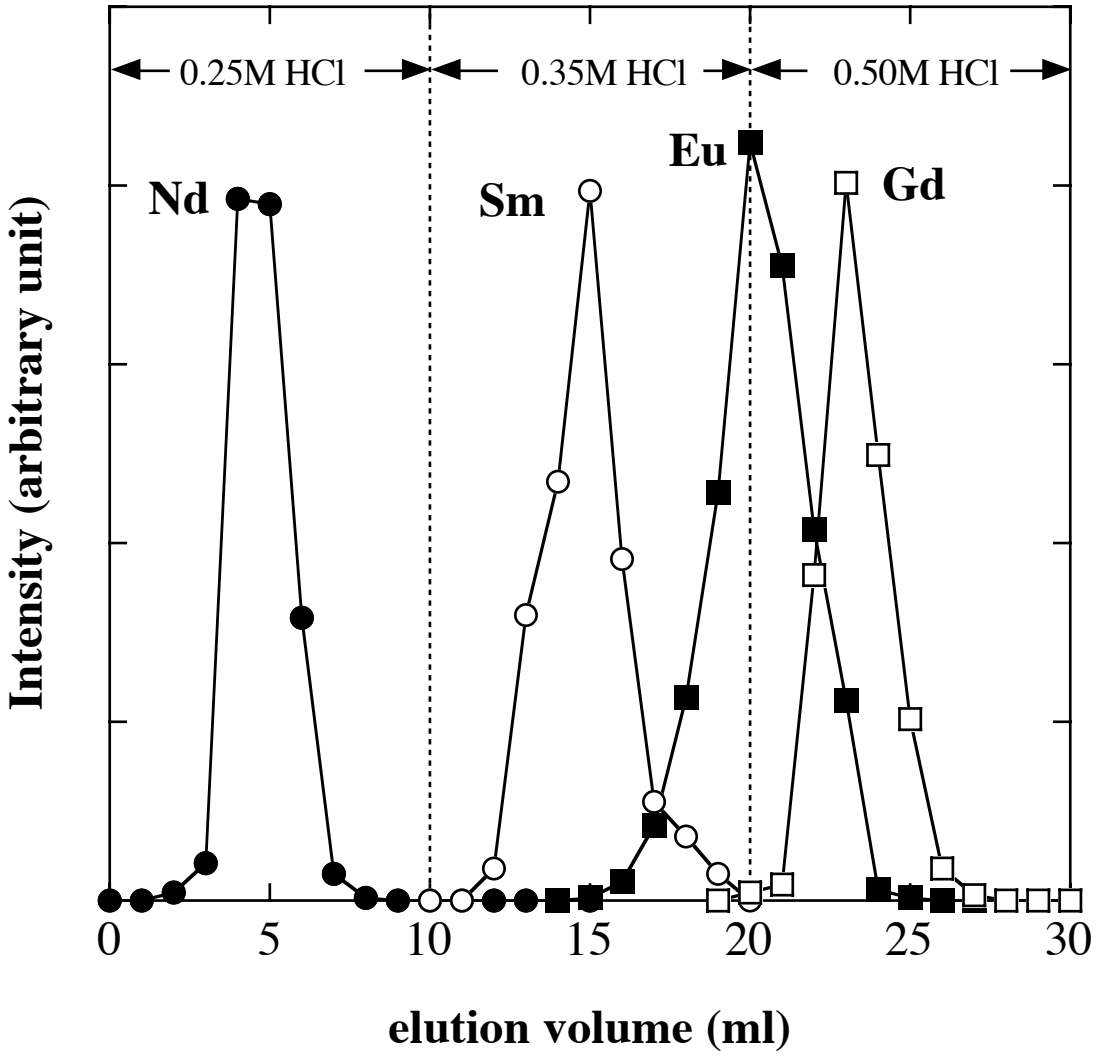

Fig. 2 Hidaka and Yoneda

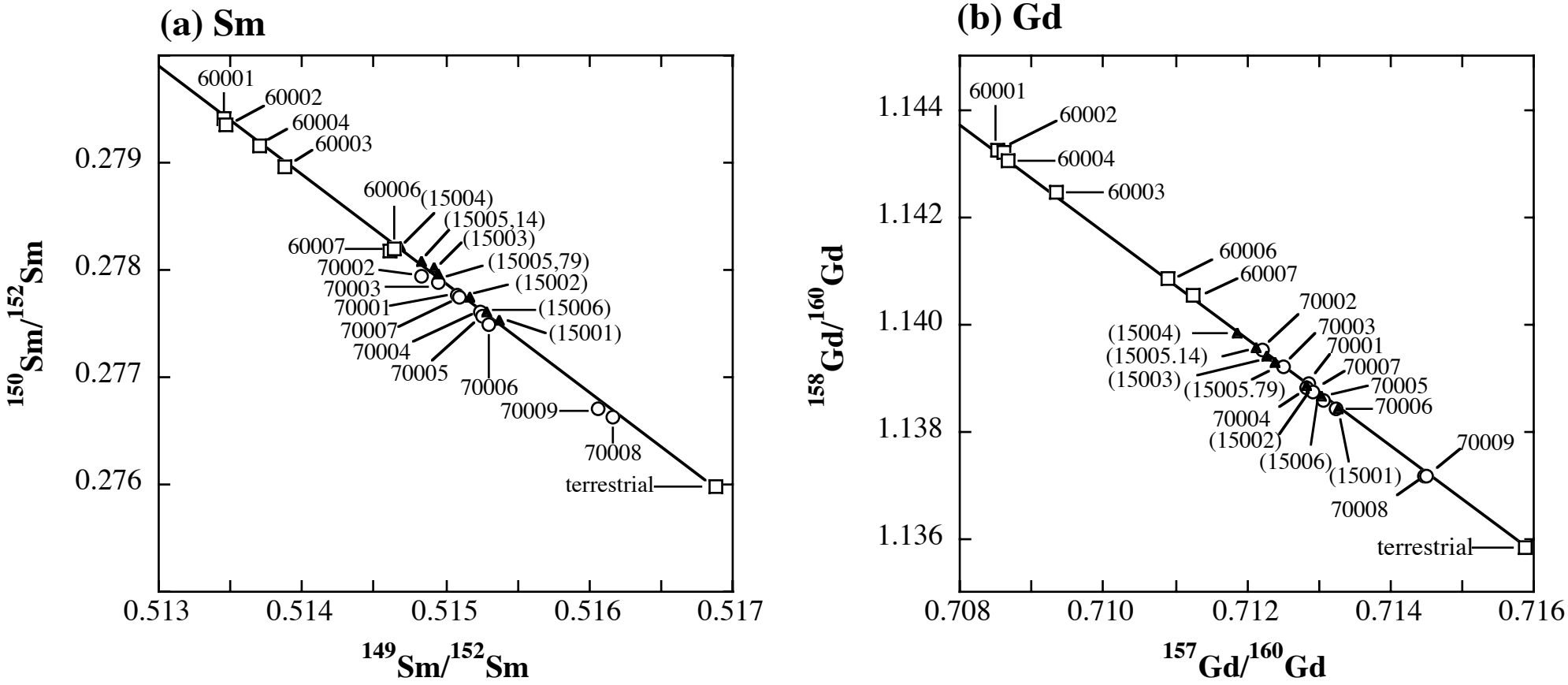

Fig. 3 Hidaka and Yoneda

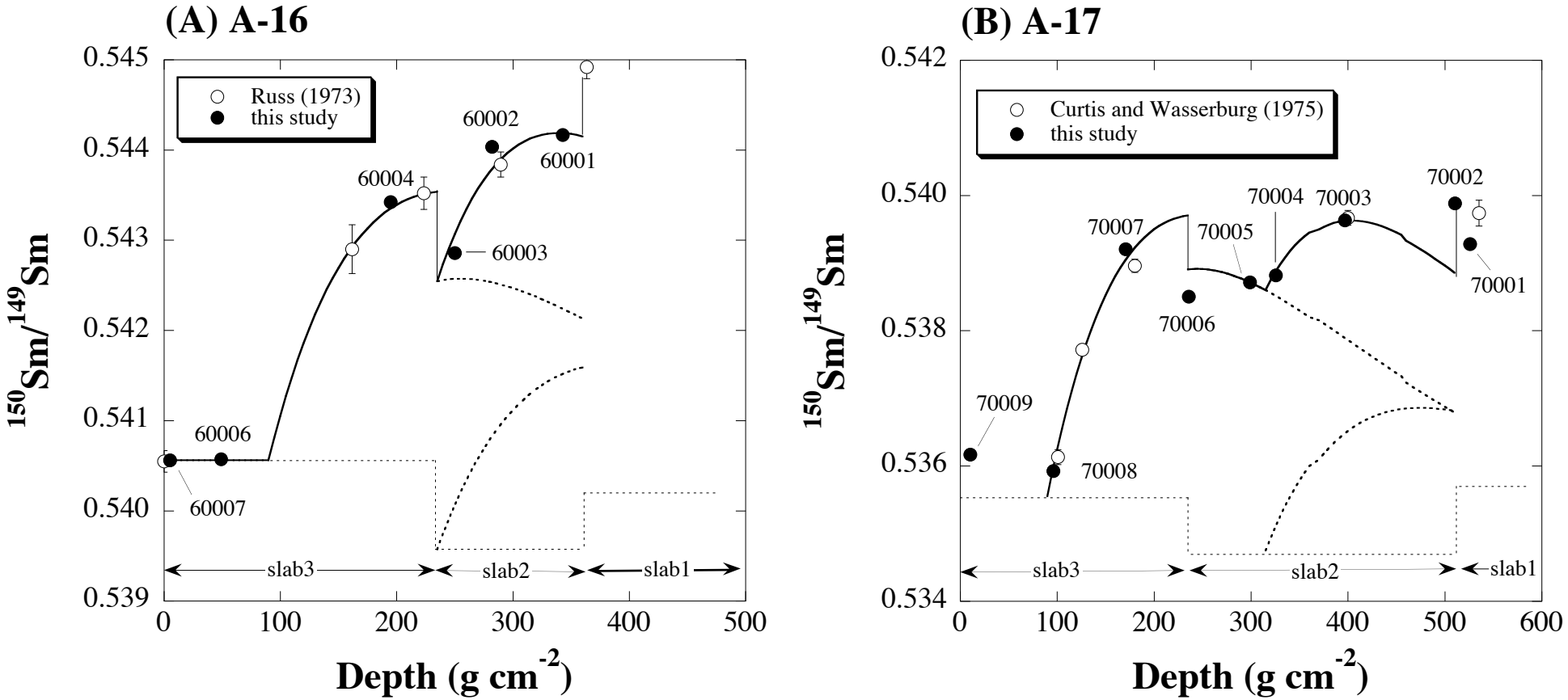

Fig. 4 Hidaka and Yoneda

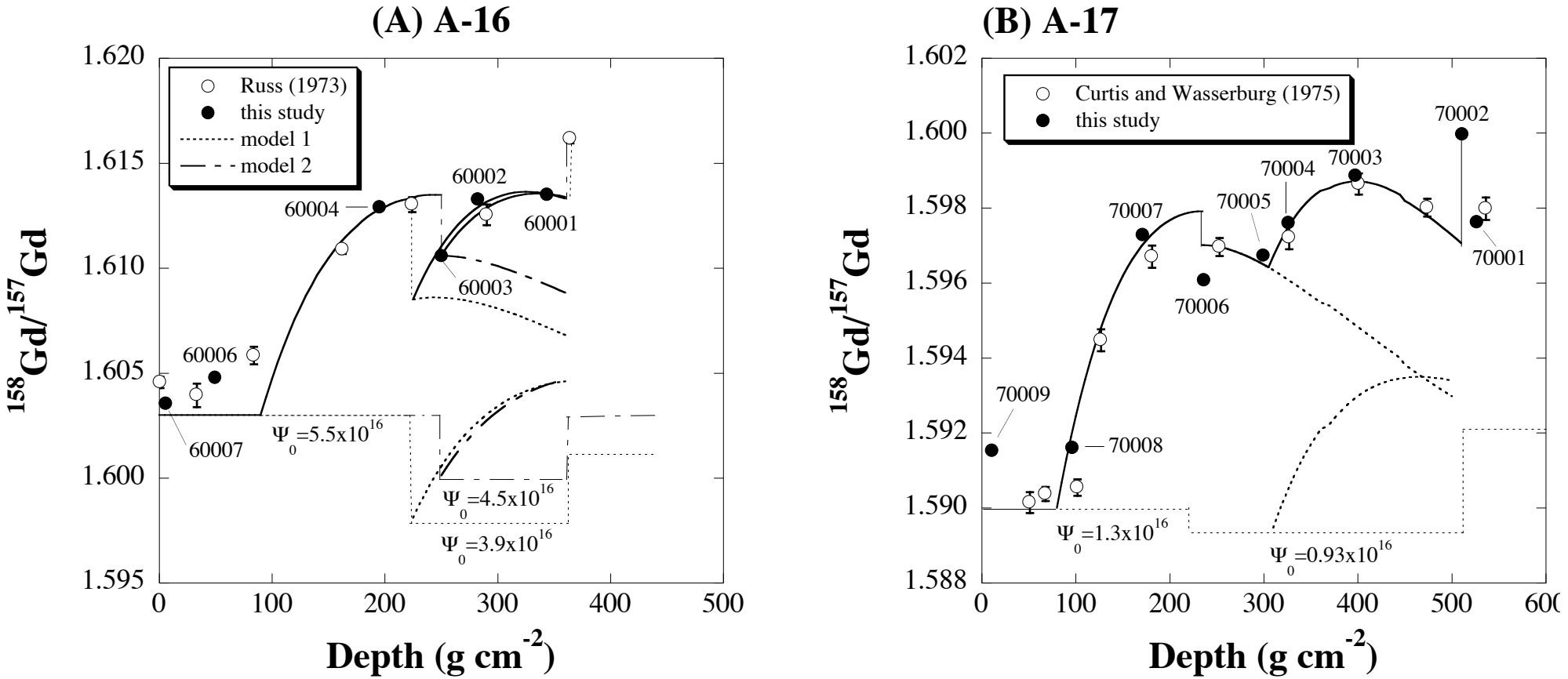

Fig. 5 Hidaka and Yoneda

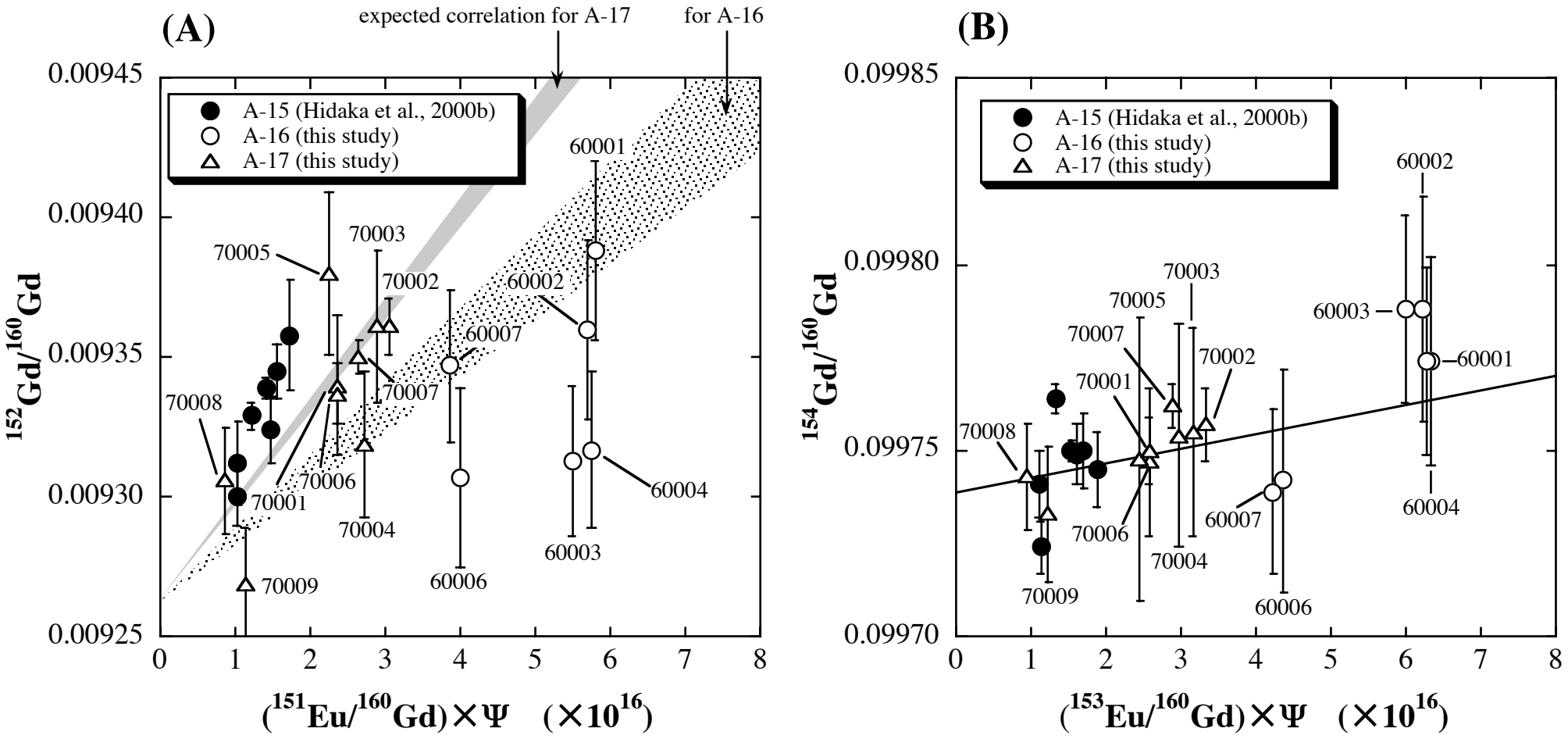

Fig. 6 Hidaka and Yoneda

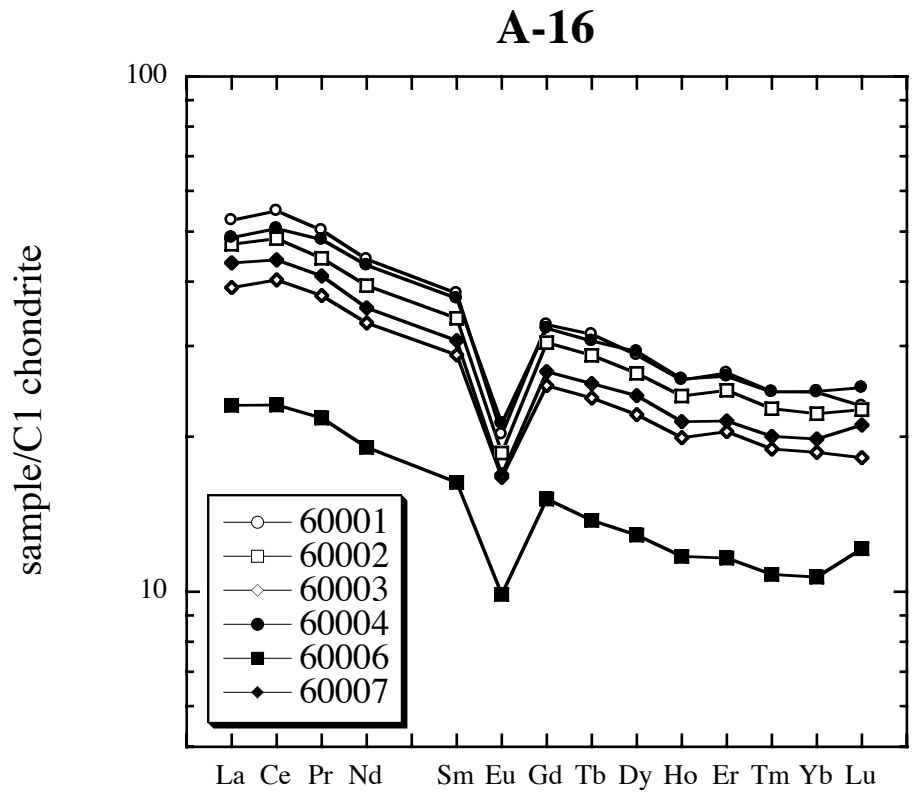

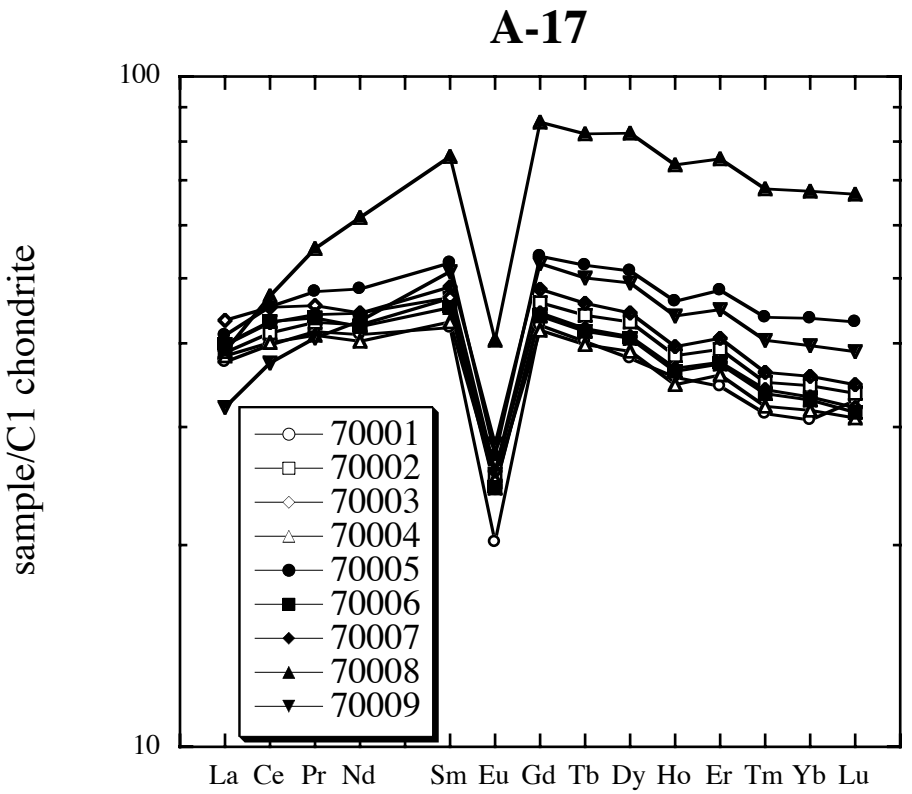

Fig. 7 Hidaka and Yoneda

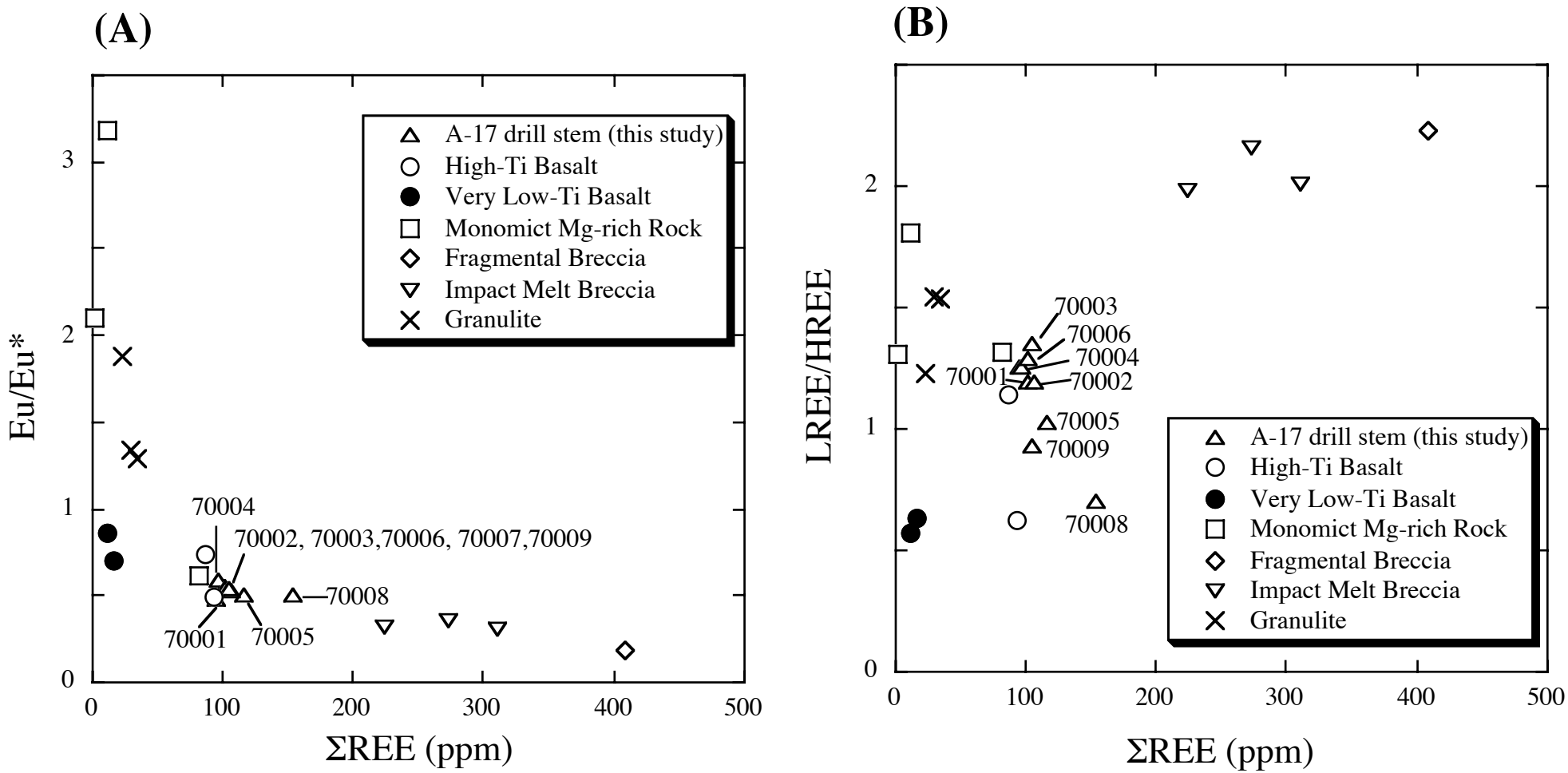

Fig. 8 Hidaka and Yoneda

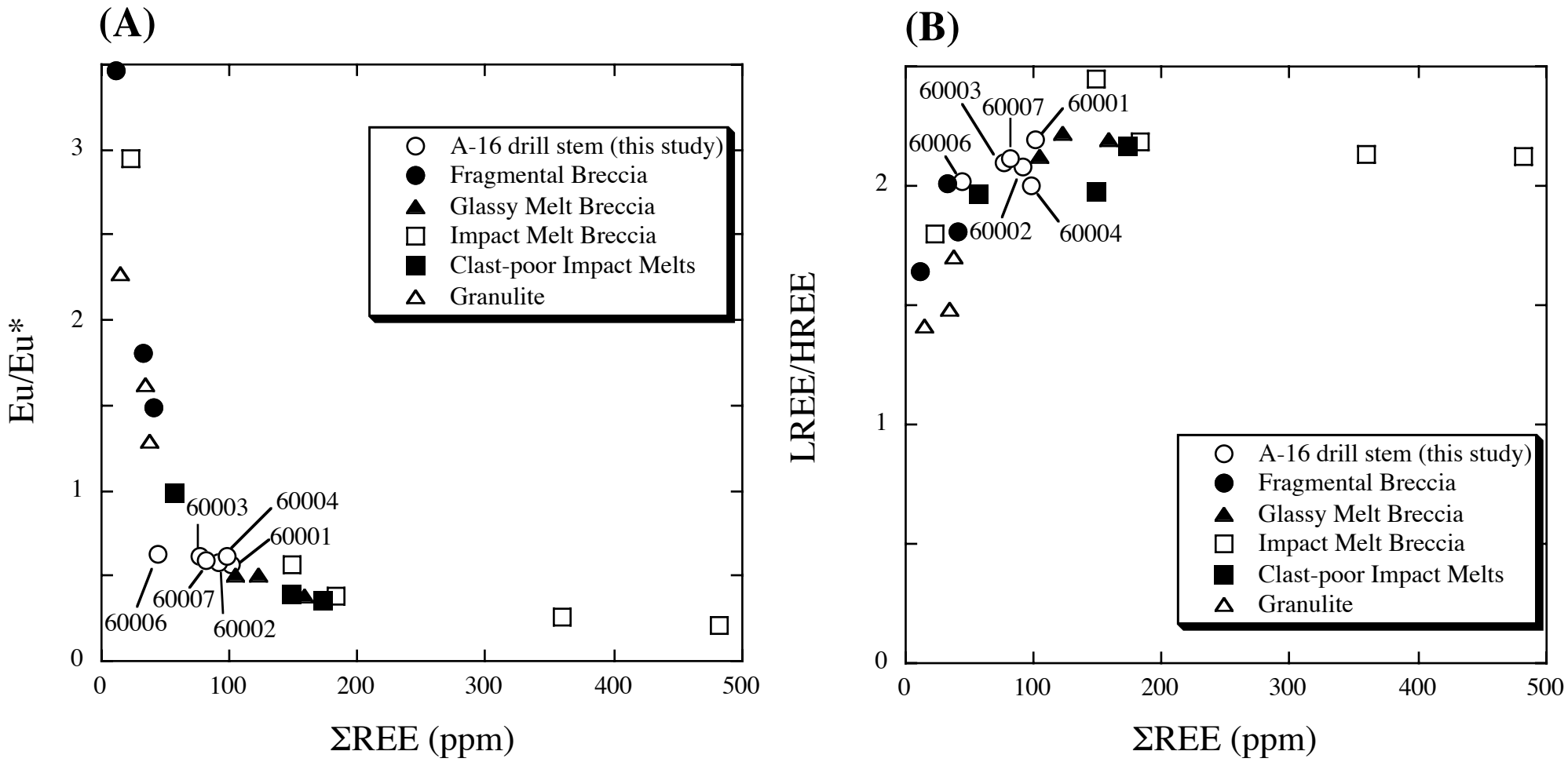

Fig. 9 Hidaka and Yoneda

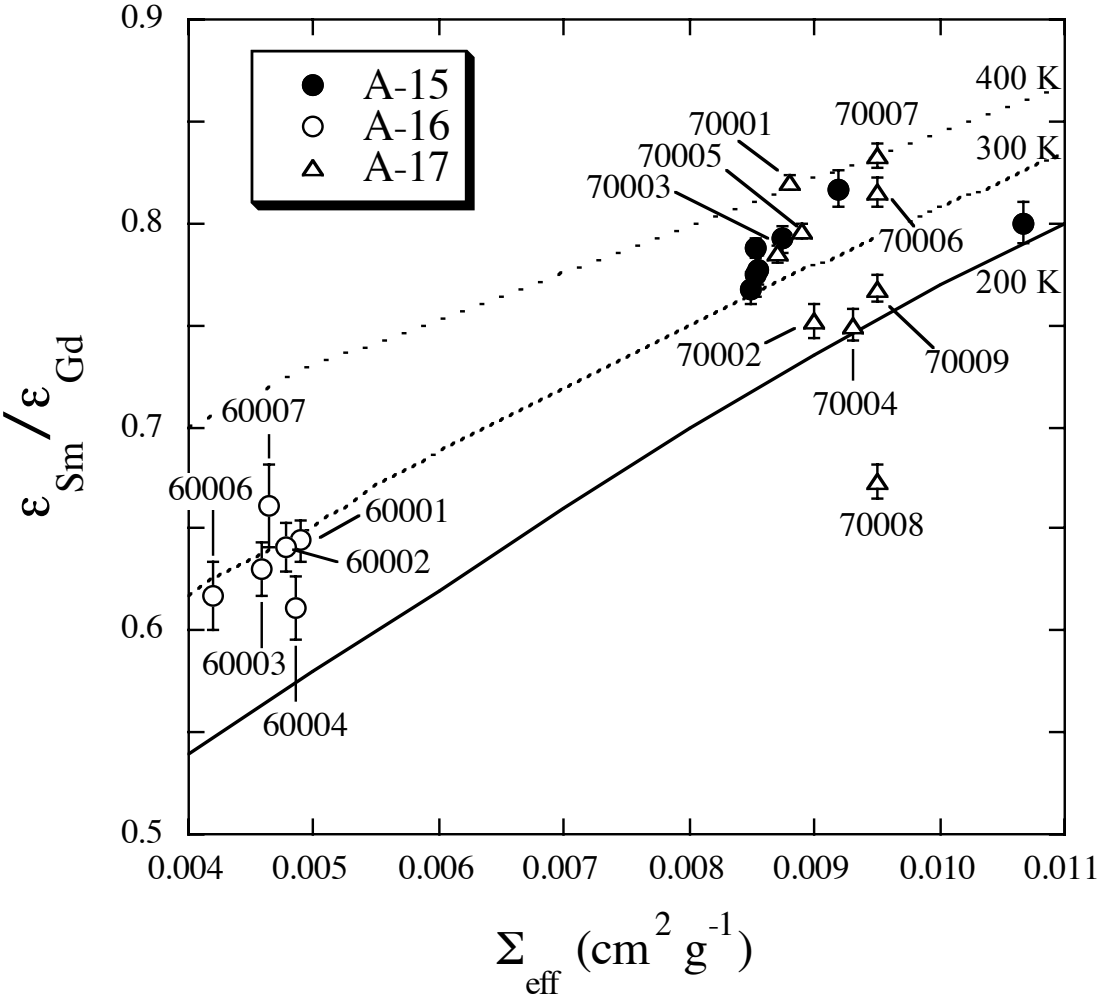

Fig.10 Hidaka and Yoneda